

An Integrated Tool for Estimation of Material Model Parameters

Sarbajit Ghosal*, Narasimha Acharya, T. Eric Abrahamson, La Moyne Porter II
SC Solutions, Inc., 1261 Oakmead Pkwy, Sunnyvale, CA 94085

Hubert W. Schreier
Correlated Solutions, Inc.

(*Corresponding author's email: ghosal@scsolutions.com)

ABSTRACT

In this paper, we present results on estimating material model parameters from inverse analysis of full-field deformation data that was obtained with a prototype of a novel integrated tool consisting of a digital image correlation system and software for data analysis and parameter estimation. Such a tool is needed for characterizing the properties of new materials, and for calibrating and validating material models. The stereo microscope-based image analysis system may be used for measurements at temperatures up to 750°C, and field sizes of approximately 1 mm. The Graphical User Interface (GUI)-based parameter estimation tool integrates modules for image data analysis and inverse analysis, and incorporates features for interfacing the tool with commercial finite element (FEM) packages. The GUI, together with a micrograph of the sample, is used to select a subset of the imaged region for analysis, and for specifying sample grain boundaries needed for developing the FEM model. Data analysis includes data averaging to reduce measurement noise, and filtering to correct for rigid body translations and rotations. The inverse analysis module runs the FEM model under experimental loading conditions within its iterative loop, using the downhill simplex method for parameter estimation. The methodology was successfully validated from measurements on a superalloy sample.

1 An Integrated Tool for Full-field Measurements and Model Calibration

In recent years, complex multi-scale material models have been increasingly used in design and analysis for various engineering applications. The scope of these physics-based models is varied, dealing with stress-strain relationships, defect initiation and growth, thermal behavior, fracture mechanics, etc. A primary purpose of attaining predictive capabilities using the material models is to estimate the performance, safety and reliability of the components that are developed using these materials, and operated under a wide range of conditions. The capabilities may be used for lifetime prediction of existing mechanical components, or for predicting the performance limits of components designed with new, engineered materials. However, for these models to be used reliably, they first need to be calibrated and validated.

A formal approach for estimation of material model parameters from experimental data was presented by Johnson *et al.* [1] with the goal of efficient model validation. This approach integrates experiments with a software platform where optimization techniques use FEM models of the sample and the data to estimate model parameters. In a typical experiment, a solid sample is subjected to a sequence of step changes in load conditions. A series of images of the sample's region-of-interest (ROI) is acquired at each load step. The images are then precisely aligned and the evolution of the displacements is calculated from the difference of each of the images relative to a reference image following extensive image analysis [1]. As shown in Figure 1, an iterative inverse analysis is required to estimate the material parameters of the model.

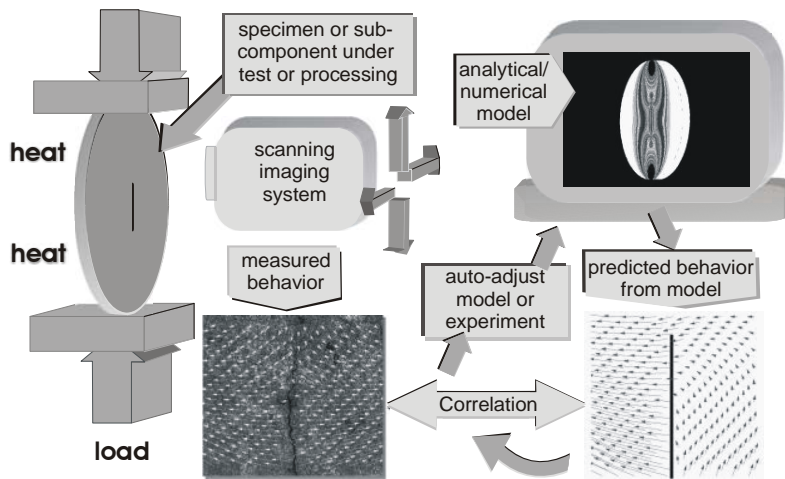


Figure 1: Schematic representing the process material model parameter estimation [1].

We have developed this concept into a novel integrated measurement, analysis, and parameter estimation tool that enables materials engineers and researchers to make deformation measurements of materials at high magnification and at high temperatures, then analyze the data, and run parameter estimation computations using commercial FEM models of the sample in an iterative procedure within the tool. In this section, we give an overview of the tool. The following sections detail results obtained for a material parameter estimation application.

The tool includes a new high-magnification stereo microscope-based Digital Image Correlation (DIC) system (Vic 3D) that can measure deformation up to temperatures of 750°C with sub-micron resolution. DIC is a non-contacting measurement technique widely used in experimental mechanics to acquire full-field deformation measurements [2]–[6]. The technique uses a random dot pattern applied to the test article to track the deformation on the surface (see Figure 2). During the experiment, images are taken at intervals, and digital image correlation is then used to determine the deformation in the image plane. A calibration is performed in order to relate the displacements found in the image plane to object displacements. The calibration permits a three-dimensional reconstruction of the object shape, as well as the determination of the complete, three-dimensional displacement vector field.

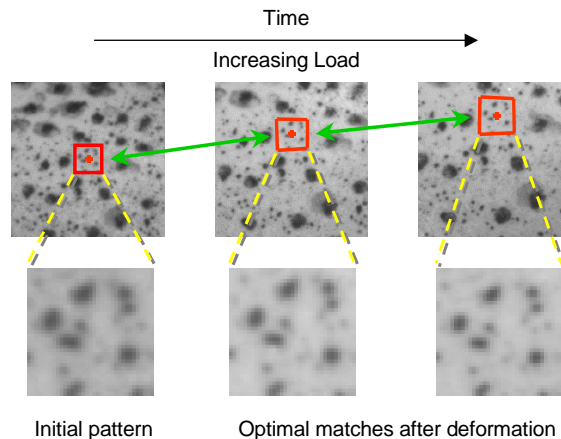


Figure 2: Tracking of object deformation using Digital Image Correlation.

The underlying concept of DIC is the measurement of displacement (and possibly displacement gradients as well as higher-order terms) at a point in an image by considering the gray value pattern in a small neighborhood. Given a second image, the objective of the method is to find the displacements (and possibly higher-order terms) that maximize the similarity between the pattern in the original image neighborhood and a displaced (and possibly deformed) version of the same pattern in the second image. An efficient method to solve this problem is the iterative algorithm proposed originally in [3]. Let θ be a parameter vector that contains the image displacements and possibly higher-order terms. Let f_i denote the gray values in the original image neighborhood, and $g_i(\theta)$

denote the corresponding gray values in the image *after* deformation. An objective function, \mathbf{E} , is defined and minimized using standard numerical methods to obtain the best parameter estimate, $\hat{\theta}$.

$$\mathbf{E} = \sum_i (f_i - g_i(\theta))^2. \quad (1)$$

The objective function could be based on the sum of the squared differences as shown above, or could use the normalized cross-correlation as well as the zero-mean normalized cross-correlation criteria for improved performance. The resolution capabilities of the DIC method have been shown to be better than 0.01 pixels for displacements with negligible bias [5], [6]. Since the digital image correlation method acquires displacement and strain data over the entire specimen area being imaged, it is ideally suited to measure non-homogeneous deformation fields.

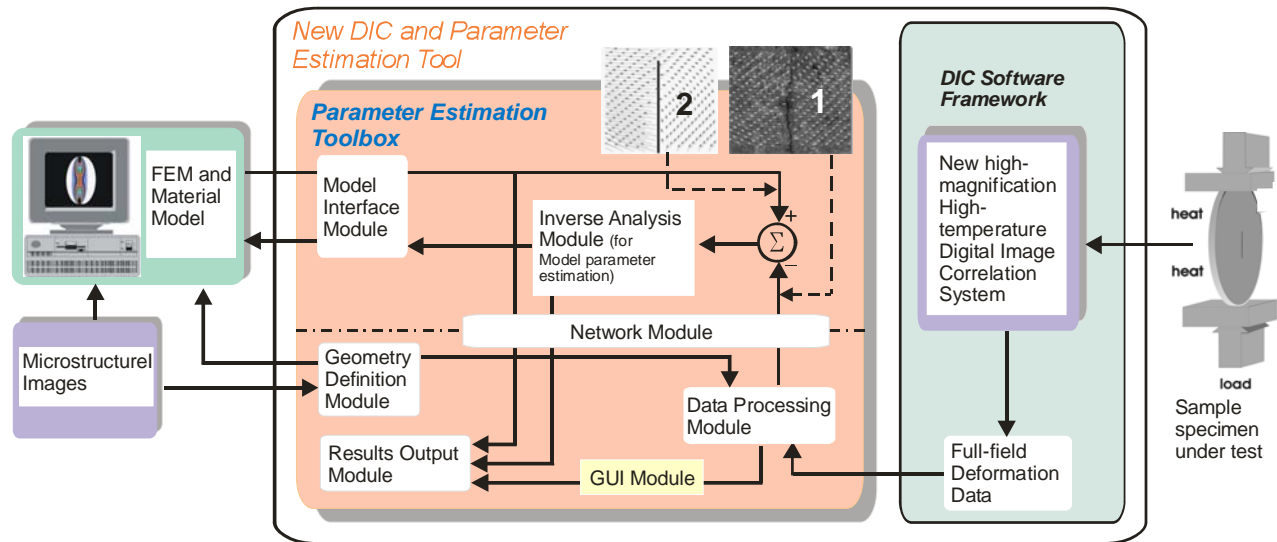


Figure 3: Schematic overview of the tool prototype. The images 1 and 2 show the deformation fields from FEM computations and the DIC data, respectively.

Figure 3 shows a high-level schematic of the integrated tool. The deformation data produced by Vic 3D is an input to the Parameter Estimation Toolbox (PE Tool), which consists of seven functional modules that exchange data (mostly through files) as shown by the arrows in Figure 3, and are related as follows:

- The *Model Interface Module* implements a protocol for exchanging data with the user-created FEM model (using third-party software) of the sample that, in turn, incorporates the material model.
- The *Geometry Definition Module* allows the user to interactively identify the grain boundaries in the form of polygons using a digital image of the microstructure, and also specify regions that the user wishes to exclude from the parameter estimation computations, e.g., if the deformation data in those regions is not sufficiently accurate.
- The *Data Processing Module* performs extensive pre-processing of the data from Vic 3D (including data averaging, transformations, etc.) to allow the user to manage the large amounts of deformation data from Vic 3D.
- The *Inverse Analysis Module* uses optimization algorithms to determine the optimal values of the material model parameters that minimize the difference between the measured and the model-predicted displacements while running the FEM model in an iterative loop.
- The *Results Output Module* incorporates several file manipulation and plotting routines to graphically display results of data analysis and parameter estimation computations.
- The *Graphical User Interface (GUI) Module* serves as the interface to all the other modules, and it integrates the various modules into one user-friendly tool. It enables the user to develop, control, and examine the results of data processing and the parameter estimation process on a Windows desktop.
- The *Network Module* allows the user to optionally perform the computationally-intensive inverse analysis on a different high-performance computer (referred to as target computer) while controlling the task using the GUI Module from the Windows “host” machine. The data and the results being

generated are available to the user for interaction and visualization purposes *via* the GUI. In Figure 3, the dot-dashed line separates the software modules that run on the host and target computers.

The integrated hardware-software tool is innovative in many ways. The high magnification stereo-microscope system permits deformation measurement with sub-micron resolution. The furnace with optical access enables measurements at high temperatures using the stereo microscope. The parameter estimation software has been designed to be modular and can be adapted to various applications easily. For example, the PE Tool can be interfaced with a wide range of commercial FEM packages and various data formats. It can incorporate new optimization techniques, and can use deformation data from multiple sources.

2 Experiment and Data Analysis

As a demonstration of the tool, deformation measurements under tensile loading were performed on a dogbone sample made of single-crystal nickel superalloy. The dogbone dimensions were 50 mm (length) by 8 mm (width, 3 mm in the neck region) by 1.5 mm (thickness), as shown in Figure 4. The rectangular measurement area of dimension 6.5 mm by 2.7 mm was located at the center of the sample on one surface. The Bunge-Euler angles, Φ_1 , Ψ and Φ_2 , were used to characterize the orientation of the crystal axis of the single-crystal sample. Sequential rotations about the laboratory coordinate axes (or the primary axes of the sample) bring the former into alignment with the principal crystallographic directions. The values of these angles were measured separately as $\Phi_1 = 8.6^\circ$, $\Psi = -3.2^\circ$ and $\Phi_2 = -8.3^\circ$.

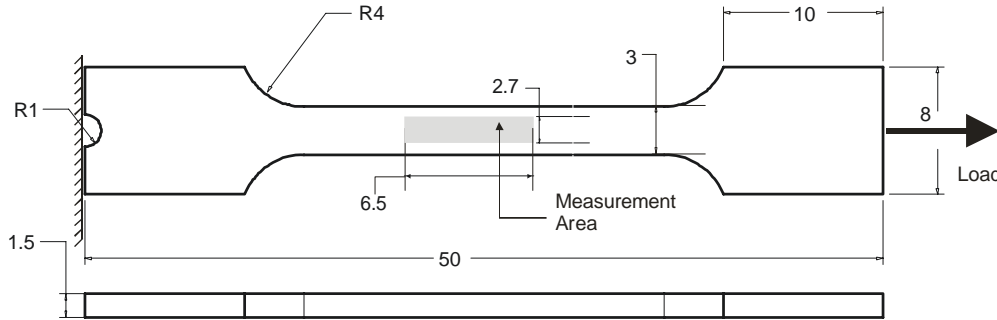


Figure 4: Schematic of the dogbone sample of the single crystal nickel superalloy showing the loading arrangement and measurement area. All dimensions shown are in mm. The schematic is not drawn to scale.

In the experiment conducted at room temperature, 240 image pairs were acquired before specimen failure, resulting in approximately 1.4 GB of image data. Image processing using the Vic-3D stereo image correlation software yielded approximately 60,000 data points per load step. However, for parameter estimation, we need deformation data at each mesh point in the measurement region of the FEM model (as described in Section 3.1). To this end, the DIC data was averaged at each mesh point using an exponential weighting function whose shape is specified by the user. There were 1071 mesh points in the FEM model of the sample, and the deformation at each of these points was obtained by averaging data at about 50–200 data points in the immediate neighborhood. The averaging also reduced the measurement noise significantly, especially for small deformations. The averaged data was then filtered to remove rigid body translation and rotation using the following filter *at each load*:

$$F = \begin{cases} u + u_0 - u_{left_edge} \\ v + v_0 - \text{mean}(v) \\ \min_{\theta} \left| R(\theta) \begin{bmatrix} u \\ v \end{bmatrix} \right|_{y=0} \end{cases} \quad (2)$$

Here, u_0 and v_0 are the offsets to account for initial deformation measurements with non-zero loading. The third operation is the rotational transformation which corrects the rigid-body rotation. We will refer to the filtered displacement data as u_f , v_f and w_f . The profiles of v and v_f are shown in Figure 5. In order to use deformation data at *all loads* for *each mesh point*, we computed the best-fit linear fit to the load-displacement graph in the elastic region, and used the slope of this line in our inverse analysis. In the process, we further reduced the effect of measurement noise.

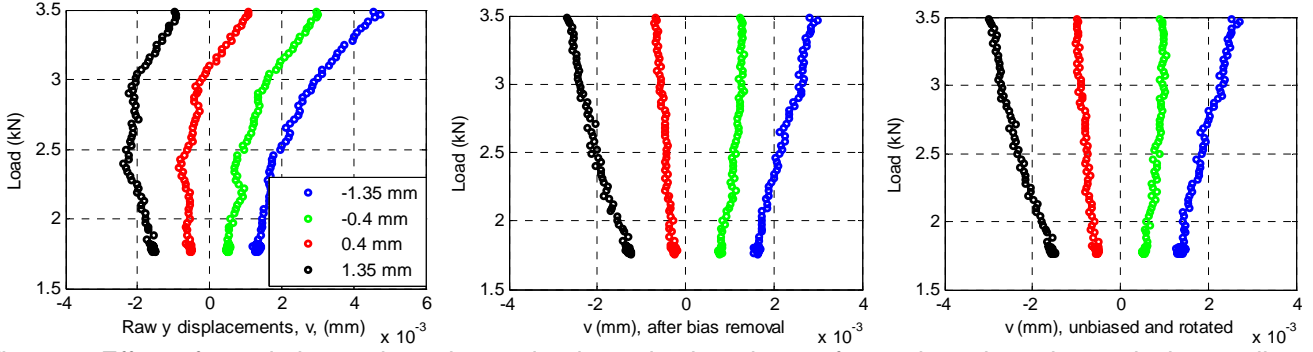


Figure 5: Effect of translation and rotation on load vs. elastic v data at four points along the vertical centerline of the sample. **Left:** raw data. **Center:** data after the mean value of v has been subtracted. **Right:** final filtered data, v_f , after performing rigid body rotation on data from the second figure.

For the plastic deformation data we found that the filtering could not adequately correct the distortions in the y -displacements (v_f) as seen in the set of graphs on the left side of Figure 6, perhaps because of minor twisting and/or bending of the sample due to loading asymmetry that is magnified at higher loads. However, it was found that the *change in the width* of the measurement area, δv , averaged over all the x locations, was less sensitive to small twisting and/or bending of the sample, as shown in Figure 6, and this metric was used for inverse analysis instead of v_f . As described in Section 3.3, the non-linear plastic region was approximated by three linear zones. As in the case of deformation in the x direction, we computed the slope of the best linear fit to the graph of the normalized load, F' vs. scaled average change in width of the measurement area, $\delta \bar{v}'_o$, which are defined as:

$$F' = \frac{F - F_1}{F_2 - F_1}; \quad \delta \bar{v}'_o = (\delta \bar{v}')_F - (\delta \bar{v}')_{F=F_1}. \quad (3)$$

Here, F_1 and F_2 are the loads at the beginning and end of each plastic region. The scaled change in width at any load with the offset, $(\delta \bar{v}')_F$, was calculated as:

$$(\delta \bar{v}')_F = \frac{(1/n_x) \sum_x \left[(v_f)_{y=y_{\min}} - (v_f)_{y=y_{\max}} \right]}{\max \left((1/n_x) \sum_x \left[(v_f)_{y=y_{\min}} - (v_f)_{y=y_{\max}} \right] \right)}. \quad (4)$$

Here, n_x is the number of points along the x direction at which the change in width was computed (51 in this case). Scaling ensures that the slopes have magnitudes of the order of unity instead of very large values that may be obtained with unscaled loads and changes in width. As before, using the slope of F' vs. $\delta \bar{v}'_o$ in inverse analysis enables use of data at all loads at a mesh point, and also reduces the effect of measurement noise.

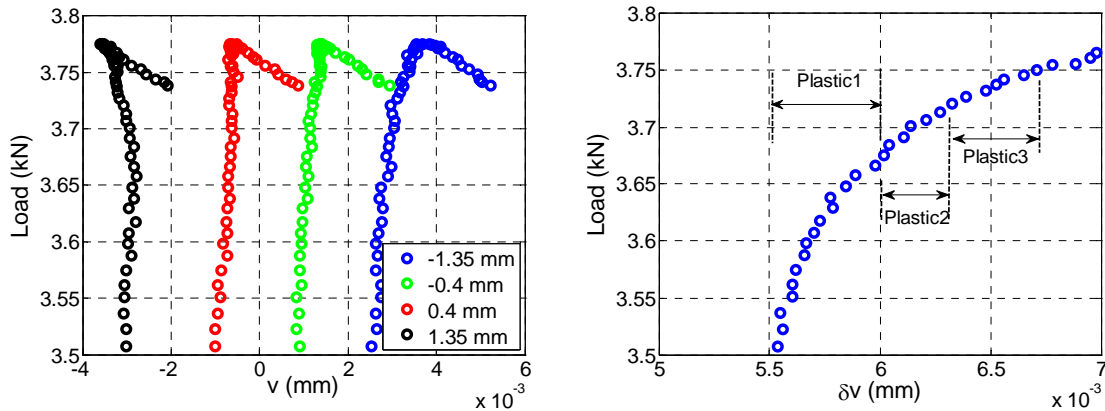


Figure 6: **Left:** Load vs. filtered y -displacements, v_f , at $x = 0$ and four y locations, **Right:** Load vs. width change averaged over 51 points along the x axis. Both figures are in the plastic region.

3 Finite Element Analysis and Material Models

3.1 Geometry, Mesh, and Boundary Conditions

We developed a 3D FEM model in ADINA[®], a commercial software product, for the dogbone sample. The mesh used consisted primarily of quad bricks, and the total number of mesh points was 9894. The measurement area was meshed separately from the rest of the dogbone with a rectangular grid of 51×21 points along the x and y axes. This separate meshing was performed to obtain a higher mesh density in the measurement area, as shown in Figure 7. One end of the dogbone was fixed (boundary conditions: fixed u , free v and w) while the other face had force boundary conditions (equal forces at all the nodes on that face that add up to the total applied force, and free u). Additionally, v and w were fixed on the end points of the longitudinal centerline on one surface.

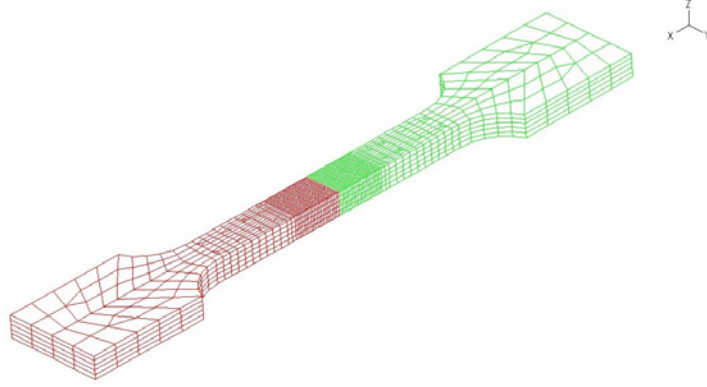


Figure 7: FEM model of dogbone sample (made of the single-crystal superalloy) developed in ADINA[®].

3.2 Elastic Region

The single-crystal superalloy has been modeled as a simply orthotropic material, with the following stress-strain relationship in the primary (material) coordinate system [7]:

$$\begin{bmatrix} \bar{\sigma} \\ \bar{\tau} \end{bmatrix} = C_{ij} \begin{bmatrix} \bar{\varepsilon} \\ \bar{\gamma} \end{bmatrix} \quad (5)$$

Here, the elasticity stiffness matrix, C is a 6×6 matrix. For *simply* orthotropic materials, only 6 out of the 36 elements are independent: $E_1(=E_2)$, E_3 , G_{12} , $G_{23}(=G_{13})$, ν_{12} , $\nu_{23}(=\nu_{13})$.

3.3 Plastic Region

The non-linear plastic region was modeled as three piecewise-linear regions, as shown in Figure 8, which displays load vs. u that was measured on the single-crystal sample at the center of the measurement region. The three locally-linear regions are marked Plastic1, Plastic 2 and Plastic3, with end-points corresponding to loads of 3.68 kN, 3.72 kN, and 3.75 kN, respectively. The deformation continues to increase with small increases in load, and additional locally linear regions can be identified. However, for purposes of demonstration of the parameter estimation technique, we will restrict ourselves to three zones. We assume that the sample does not undergo creep, *i.e.*, that the strains are only dependent on the load and are time-independent at a given load.

Hill's model was used for yield and a hardening rule was used for deformation in the plastic region. The Hill's yield model has six parameters which are the yield stresses in the directions of the material axes (1, 2, 3) and the yield stresses for pure shear in the material planes (12, 23, 13), *i.e.*, $\sigma_{Y,1}$, $\sigma_{Y,2}$, $\sigma_{Y,3}$, $\sigma_{Y,12}$, $\sigma_{Y,23}$, $\sigma_{Y,13}$, respectively. We used a single universal plasticity modulus, E_u^p for modeling hardening [8]. Effective Poisson ratios along the material axes (denoted by subscripts 1, 2, and 3) were used, and these are related *via* Lankford coefficients, (r_0 , r_{45} , r_{90}), and volume conservation [9]. In ADINA[®]'s implementation of this plasticity model, there are five independent parameters: $\sigma_{Y,1}$, r_0 , r_{45} , r_{90} , and E_u^p . Hence, a set of Lankford coefficients is needed for each of the three linear segments that approximate the plastic region. Of course, the relationship to yield stresses *via* the Hill parameters is physically meaningful only for the first linear plastic zone.

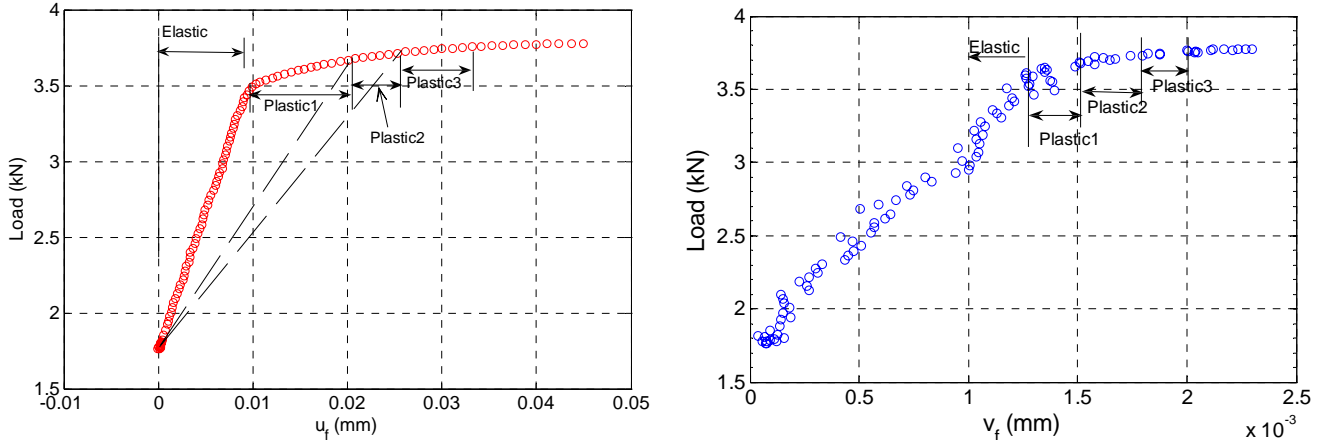


Figure 8: **Left:** Load vs. u data at the center of the measurement region for the single-crystal sample. **Right:** Load vs. v data at $x = 0$, $y = -1.35$ mm for the single-crystal sample.

4 Parameter Estimation for the Elastic Region

In the inverse analysis for parameter estimation, the generalized cost function, J , that was used in the optimization computations was defined as the two-norm of the normalized error between the model prediction and the experimental values of Y , averaged over the total number of measurement axes (n) and FEM models (m). Here, Y may represent either the (filtered) measured displacements, or the best-fit slope of the load vs. displacement graph:

$$J = \frac{1}{m} \sum_{i=1}^m \left[\frac{1}{n} \sum_{j=1}^n \left\{ \sqrt{\frac{1}{N} \sum_{k=1}^N W_{i,j,k} \left\| \frac{Y_{E,i,j,k} - Y_{M,i,j,k}}{Y_{E,i,j,k}} \right\|^2} \right\} \right]_j \quad (6)$$

The subscripts E and M refer to the experimental data and model results, respectively. The number of good data points (i.e., mesh points where the displacement measurements are sufficiently accurate) in the i^{th} model along the j^{th} axis is N_{ij} . Since we are using only one FEM model, $m = 1$. Also, since we are not using w data, $n = 2$. Each data point has a weight $W_{i,j,k}$ that can have any value between 0 and 1.

When we analyzed the sensitivity of the measurements to the material model parameters, it was found that only two of the six parameters in this simply orthotropic model showed sensitivity to the measured displacements, and hence only these two ($E_1 = E_3$, E_2) could be estimated. The reason for this limitation is two-fold. First, since the sample motion in the out-of-plane direction was not very well constrained during the test, the out-of-plane deformation data, w , did not contribute meaningful information for parameter estimation. Second, for small values of Bunge-Euler angles, as is the case for this sample (see Section 2), the principal stresses in the material coordinate system, σ_2 and σ_3 have very small magnitudes. Consequently, the dependence of u and v on material parameters other than E_1 and ν_{12} (through elements of the matrix C_{ij}) is very weak. The situation would be different if the material axes were to be substantially out of alignment with the global coordinate axes, in which case the stress vector would be full, and the measured displacements (consequently, the cost function J) would have significant sensitivity to all the material parameters.

Inverse analysis was performed using the downhill simplex method, a robust search algorithm that has been successful in finding the global minimum of various non-linear cost functions, and does not involve slope computations [10]. Table 1 shows the values of the elastic Young modulus along the (1, 2) material axes that were obtained after starting from two different sets of trial values that are quite far apart. Figure 9 shows the load vs. displacement (v_f) graphs from the FEM model using these optimal parameters and with the data. Good agreement between the model and data is seen in the elastic range. For the other four parameters, we used nominal values for this material of $\nu_{12} = \nu_{13} = 0.39$, $\nu_{23} = 0.3$, $G_{12} = G_{13} = 100$ GPa, $G_{23} = 110$ GPa. The values of E_1 and E_2 obtained here compares well with the effective modulus of 138.3 GPa in the loading direction calculated from the gross measurements. The optimization computations took approximately half an hour to converge on a

Linux workstation powered by an AMD Opteron 248 running at 2.2 GHz with 12 GB of RAM machine. Almost all of the computation time is used for the cost function computations, i.e., running the ADINA® simulations.

Table 1: Optimal parameters for the elasticity model.

	Run 1		Run 2	
	Initial	Final	Initial	Final
E_1 (GPa)	80.0	129.5	180.0	129.5
E_2 (GPa)	80.0	141.6	180.0	141.6

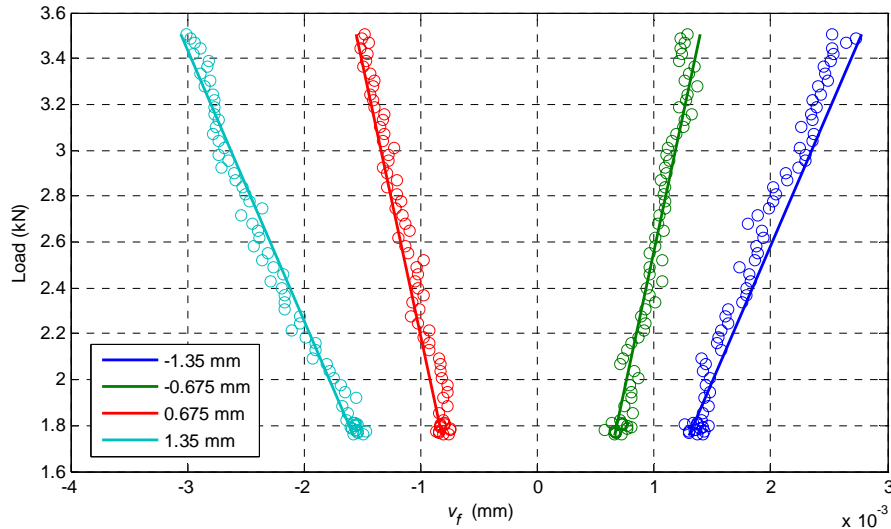


Figure 9: Load vs. v_f at four points along centerline ($y = 0$) in the elastic regime. Circles are experimental data and the straight lines are FEM model results for optimal material parameters.

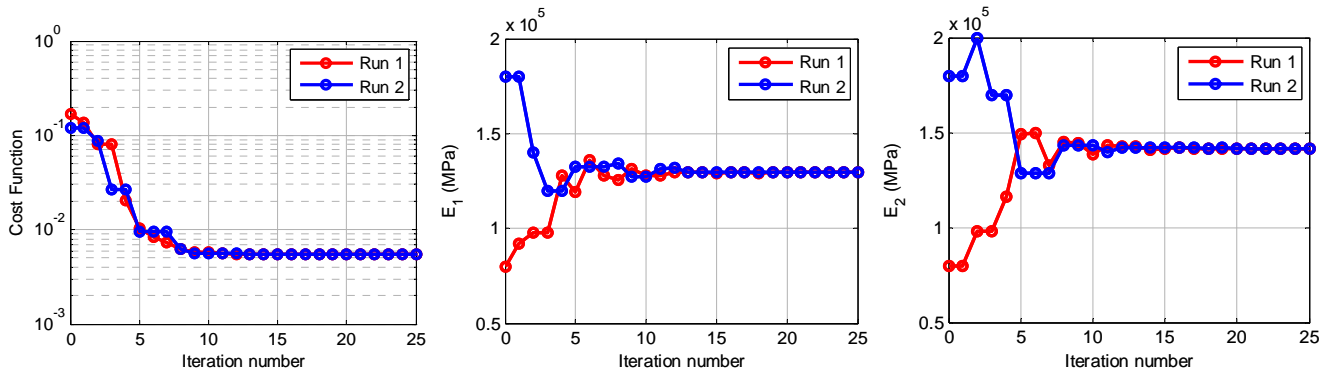


Figure 10: Convergence plots for the estimated material parameters of the single crystal sample, and the associated cost function..

5 Parameter Estimation for the Plastic Region

As stated earlier, we have modeled the plastic region as consisting of three piece-wise linear segments (denoted as Plastic1, Plastic2 and Plastic3 in Figure 8), each with its own universal plasticity modulus and Lankford coefficients. We first estimate the parameters for Plastic1 zone. The elastic properties are specified as the values determined from the elastic analysis of Section 4. In order to implement the model for plastic zones 2 and 3, we assume that the boundary point between zone 1 and 2 is the yield point of a fictitious material with elastic properties, as shown using dotted lines in Figure 8. Next, we estimate the elastic properties of this fictitious material, and the plastic properties (yield stresses, universal plasticity modulus and Lankford coefficients). We discard the elastic properties and the yield stresses and retain the Lankford coefficients and the universal plasticity modulus for the zone Plastic2. This procedure is then repeated for the third plastic zone.

Sensitivity analyses showed that for this single crystal sample under the imposed loading condition, we can estimate only three of the five material model parameters: $\sigma_{Y,1}$, r_0 , and the universal plasticity modulus, E_p^u . The other two coefficients were assigned the following values: $r_{45} = 0.2$ and $r_{90} = 0.05$. These approximate values were determined from the measured strain ratios in the three directions. The plasticity model involves both the yield stress and hardening behavior model parameters (Lankford coefficients). Consequently, in our linearized (slope-based) approach to the plastic zone, we have to tie down the plasticity slope to the yield point. Therefore, the cost function was modified to incorporate the error in the displacements at the yield load. The cost function, J , was re-defined for the plastic zones as:

$$J = \frac{\sum_{j=1}^2 \sum_{k=1}^N \left\| \frac{Y_{E,j,k} - Y_{M,j,k}}{Y_{E,j,k}} \right\|^2 + 0.25 \sum_{k=1}^N \left\| \frac{u_{f,E,k} - u_{f,M,k}}{u_{f,E,k}} \right\|^2}{2N} \quad (7)$$

Here u_f is the filtered x-displacement at yield load. This term has weighting of 0.25 to reduce the potential effect of noise in the u data on the optimization accuracy. The choice of the factor of 0.25 was reached after trying a few other values for the fastest convergence. Y is the best-fit slope to the load-displacement plot. The subscripts j refers to the axis (x or y), k represents the data point number, and E and M refer to experimental data and model results, respectively. The optimization computations took approximately 12 hours to converge for Plastic 1 zone, and 6-7 hours for the other two plastic zones on the AMD Opteron workstation running at 2.2 GHz with 12 GB of RAM.

The optimal parameters for the three plastic zones are shown in Table 2 and Table 3. Figure 11 shows the comparison of the model and data over the entire load range of interest. The figure on the left shows average stress vs. strain at two points. The quality of the model fit can be examined more closely in the graphs on the right side of Figure 11 where u_f has been plotted individually for the elastic and the three plastic zones. The fits are very good overall, and the optimization convergence is excellent (see Table 2 and Table 3).

Table 2: Initial and final parameter values for the first plastic zone.

	Run 1		Run 2	
	Initial	Final	Initial	Final
E_p^u (GPa)	10.0	13.7	18.0	13.7
$\sigma_{Y,1}$ (GPa)	0.40	0.77	0.80	0.77
r_0	0.2	0.021	0.025	0.021

Table 3: Initial and final parameter values for the second and third plastic zones.

	Plastic Zone 2				Plastic Zone 3			
	Run 1		Run 2		Run 1		Run 2	
	Initial	Final	Initial	Final	Initial	Final	Initial	Final
E_p^u (GPa)	10.0	6.4	2.5	6.4	7.5	4.74	5.0	4.75
r_0	0.2	0.061	0.25	0.061	0.25	0.064	0.1	0.064

6 Conclusions

We have successfully demonstrated the capability of a new integrated hardware-software tool to measure full-field deformation data and then process the data for use in estimating the sample's material model parameters. The stereo microscope-based DIC system can handle field sizes of about 1 mm and high temperatures up to 750°C. Measurements were made on a single-crystal nickel superalloy sample. The parameter estimation toolbox processed the vast amounts of DIC data that was generated, and interface with ADINA®, a commercial FEM software to run the model in an iterative loop during optimization calculations. The model parameters converged to the same values irrespective of the starting points, and the final values are typical of this material. It was noted that the choice of sample and the quality of the data can have a major impact on the parameter estimation results.

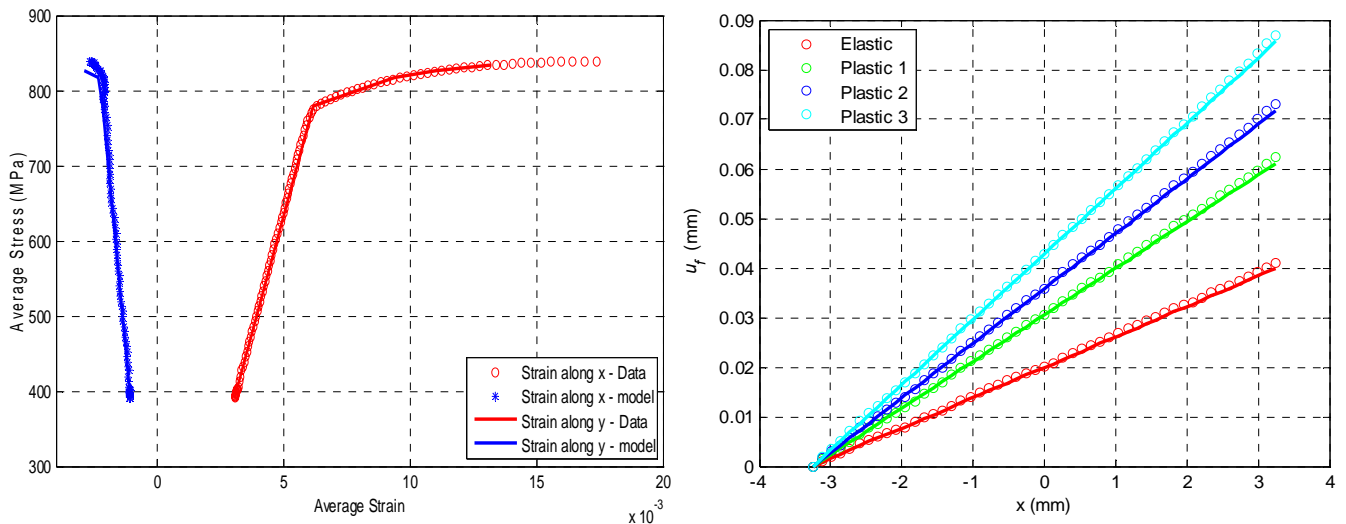


Figure 11: **Left:** Graphs of average stress vs. strain in x directions (mesh point at (3.25 mm, 0)), and y direction (mesh point at (0, 1.35 mm)). Circles are experimental data and the straight lines are FEM model results for optimal material parameters. **Right:** u_f at all points along the x direction for elastic and plastic regions with displacements in each zone shifted to pass through same starting point to allow closer inspection of the match between model and data.

Acknowledgement

This work was funded by the Air Force SBIR Contract # FA8650-05-C-7251. The authors would like to thank Dr. D. A. Johnson, Dr. R. John, Dr. M. J. Shepard, 2nd Lt. S. M. Visalli, and 2nd Lt. S. Haering at AFRL for technical discussions and for program support, as well as Prof. M. A. Sutton and A. P. Reynolds at University of South Carolina, Columbia, SC, and Dr. J. L. Ebert at SC Solutions for their technical suggestions.

References

- [1] Johnson, D. A., Porter III, W. J., John, R., "Full-Field Techniques in the Study of Multi-Scale Nonlinear Material Behavior," Proc. SEM Annual Conference, *Experimentation and Modeling at the Nanoscale*, Society for Experimental Mechanics, Charlotte, NC, 2–4 June 2003.
- [2] Chu, T. C., Ranson, W. F., Sutton, M. A., Peters, W. H., "Application of Digital Image Correlation Techniques to Experimental Mechanics," *Experimental Mechanics*, 25 (3), pp 232–245, 1985.
- [3] Sutton, M. A., Cheng, M., Peters, W. H., Chao, Y. J., and McNeill, S. R., "Application of an Optimized Digital Correlation Method to Planar Deformation Analysis," *Image and Vision Computing*, 4 (3), pp 143-150, 1986.
- [4] Helm, J. D., McNeill, S. R., Sutton, M. A., "Improved 3-D Image Correlation for Surface Displacement Measurement," *Optical Engineering* 35 (7), pp. 1911-1920, 1996.
- [5] Schreier, H. W., Braasch, J. R., Sutton, M. A., "Systematic Errors in Digital Image Correlation Caused by Intensity Interpolation," *Opt. Eng.*, 39(11), 2000.
- [6] Schreier, H. W., Sutton, M. A., "Systematic Errors in Digital Image Correlation Due to Undermatched Subset Shape Functions," *Experimental Mechanics*, 43(2), 2002.
- [7] Jones, R. M., *Mechanics of Composite Materials*, 2nd Edition, Taylor and Francis, 1999.
- [8] ADINA R&D, *ADINA Theory and Modeling Guide, Volume 1: ADINA Structures and Solids*, p. 278, October 2005.
- [9] Lankford, W. T., Snyder, S. C., Bausher, J. A., "New Criteria for Predicting the Press Performance of Deep Drawing Sheets", *Trans. ASM*, 42, 1197–1205, 1950.
- [10] Press, W. H., Flannery, B. P., Teukolsky, S. A., Vetterling, W. T., *Numerical Recipes in C, The Art of Scientific Computing*, Cambridge University Press, Second Ed., 1992.